JACS
JOURNAL OF THE AMERICAN CHEMICAL SOCIETY
Article
pubs.acs.org/JACS

The Good Host: Formation of Discrete One-Dimensional Fullerene "Channels" in Well-Ordered Poly(2,5-bis(3-alkylthiophen-2-yl)thieno[3,2-*b*]thiophene) Oligomers

Lei Zhang,[†,Δ] Feng Liu,[†,Δ] Ying Diao,[§] Hilary S. Marsh,[∥] Nicholas S. Colella,[†] Arthi Jayaraman,[⊥] Thomas P. Russell,[†] Stefan C. B. Mannsfeld,*[,‡] and Alejandro L. Briseno*[,†]

[†]Department of Polymer Science and Engineering, University of Massachusetts, 120 Governors Drive, Amherst, Massachusetts 01003, United States

[‡]Center for Advancing Electronics Dresden, Dresden University of Technology, 01062 Dresden, Germany

[§]Stanford Synchrotron Radiation Lightsource, Menlo Park, California 94025, United States

[∥]Department of Chemical and Biological Engineering, University of Colorado, Boulder Colorado 80309 United States

[⊥]Department of Chemical and Biomolecular Engineering and Department of Materials Science and Engineering, University of Delaware, Newark, Delaware 19716, United States

Supporting Information

ABSTRACT: Due to the unique crystallinity of poly(2,5-bis(3-alkylthiophen-2-yl)thieno[3,2-*b*]thiophene) (PBTTT), it is an excellent model polymer to study the structure−property relationship in organic devices, especially those relying on junctions of electron- and hole-transporting materials. Here, we report the synthesis and characterization of a series of monodisperse PBTTT oligothiophenes (n = 1−5) and systematically examine the evolution of crystalline behavior, morphology, and interaction with [6,6]-phenyl C_{61}-butyric acid methyl ester (PCBM) as the molecular conjugation length increases. We discovered that fullerene intercalation occurs when there is enough free volume between the side chains to accommodate the fullerene molecule. The intercalation of PCBM is observed beyond BTTT-2 and longer oligomers, likely similar to that of PBTTT. Interestingly, both experiments and molecular simulations show that PCBM intercalation also appears to "catalyze" a more efficient packing of the BTTT-2 dimers. Crystal structure analysis revealed that the straight BTTT-2 side chains form one-dimensional (1D) channels that could perfectly host PCBM but, in the pure material, accommodate the interdigitated side chains from adjacent layers. In the blend with PCBM, these channels are maintained and enable the cocrystallization and intercalation of PCBM. This is the first time the actual sublattice cell of PCBM has been determined from the X-ray data, and demonstration the utility of the oligomers as model systems for their polymer counterparts. Among the organic photovoltaic devices (OPVs) made from the BTTT oligomers and [6,6]-phenyl C_{71}-butyric acid methyl ester ($PC_{71}BM$) blends, the ones containing the BTTT-2 dimer exhibit the highest performance.

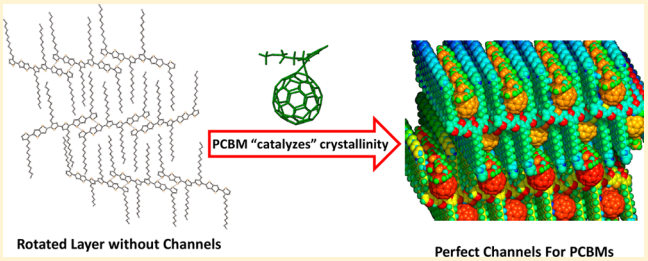

INTRODUCTION

Thiophene-based materials are some of the most investigated semiconductor materials for applications in organic electronics, due to the ability to tailor their chemical and electronic structure.[1−5] Polymers have been synthesized that show excellent charge-transport properties, which are crucial for their use in organic field-effect transistors (OFETs) and organic photovoltaics (OPVs).[6,7] While it has become increasingly clear that the morphology of these materials in the solid state is critical for their performance, charge transport is still fundamentally dependent on charge transfer at the molecular level.[8−14] Due to the high molecular weight and inherent defects of polythiophenes, single crystals are exceptionally challenging to grow, making it difficult to probe these semiconductors at the molecular level.[15]

In contrast, oligothiophenes show well-defined structures with minimal defects.[16−20] Additionally, due to the lower entropic barrier and lack of chain entanglements, oligothiophenes are significantly easier to crystallize than higher molecular weight polythiophenes.[21−25] These factors allow for the generation of single crystals that are suitable for X-ray analysis, revealing the packing of these materials at the molecular level.[21−25] Similar to the well-studied poly(3-hexylthiophene) (P3HT),[10,26,27] poly(2,5-bis(3-alkylthiophen-2-yl)thieno[3,2-*b*]thiophene) (PBTTT) exhibits high hole mobility (>0.1 $cm^2 \cdot V^{-1} \cdot s^{-1}$) in thin films.[28−30] In fact, PBTTT generally displays higher performance than P3HT

Received: October 24, 2014
Published: November 25, 2014

dx.doi.org/10.1021/ja510976n | J. Am. Chem. Soc. 2014, 136, 18120−18130

Scheme 1. Synthetic Steps to BTTT Oligomers and Polymers[a]

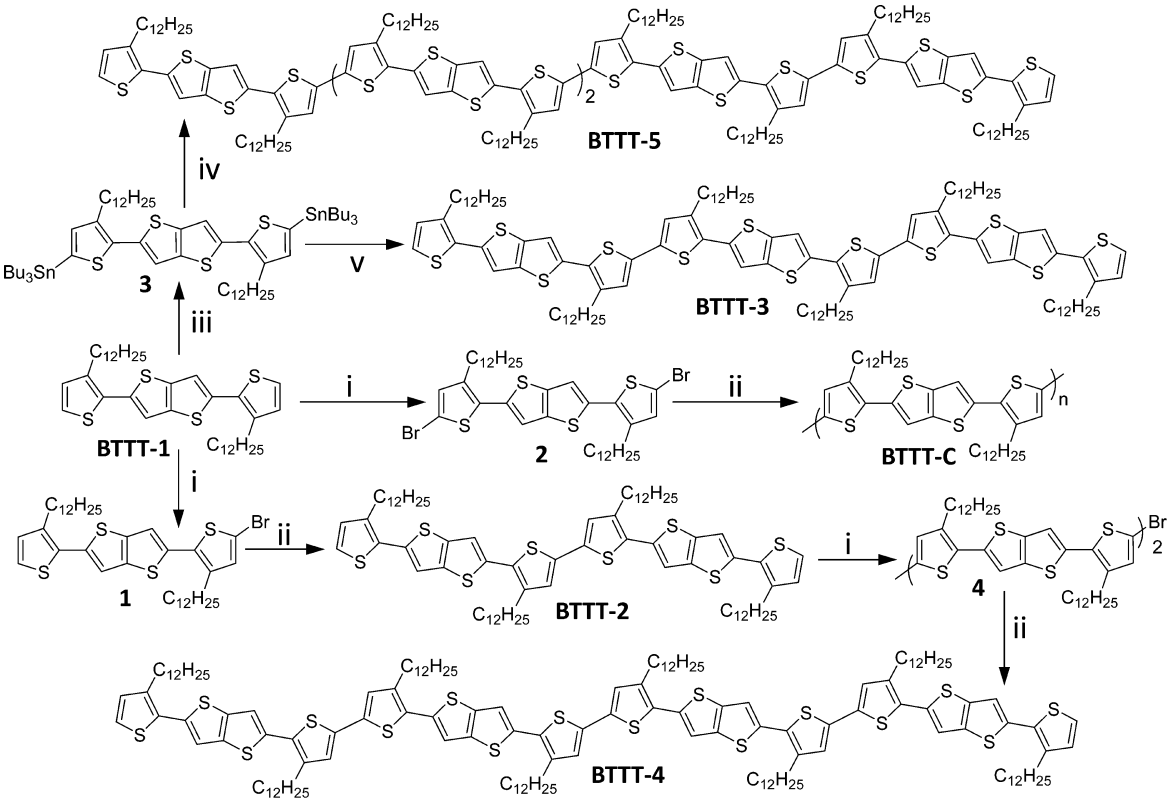

[a]Reagents and conditions: (i) NBS, AcOH/chloroform (1:1), 0 °C to room temperature; (ii) bis(tri-*n*-methyltin), $Pd(PPh_3)_4$, toluene, 115 °C; (iii) BuLi, tributyltin chloride, THF, −78 °C to room temperature; (iv) **4**, $Pd(PPh_3)_4$, toluene, 115 °C; (v) **1**, $Pd(PPh_3)_4$, toluene, 115 °C.

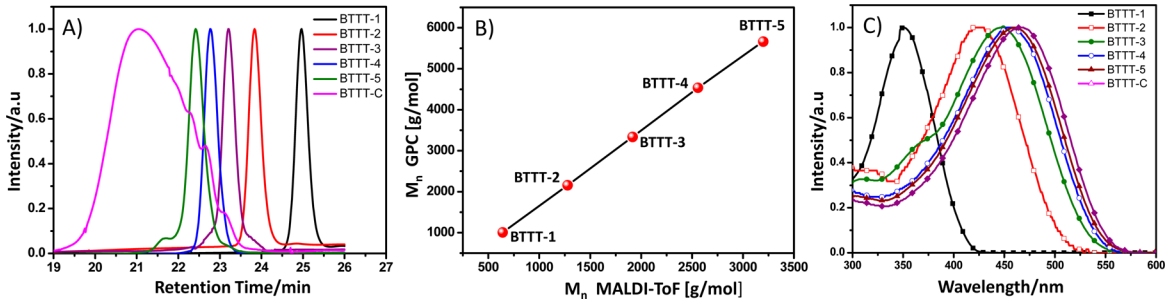

Figure 1. (A) GPC traces of oligothiophenes (in trichlorobenzene solvent vs PS standard), (B) comparison with MALDI-TOF (terthiophene as the matrix), and (C) UV−vis spectra of oligomers in chloroform solution.

due to increased crystallinity in three dimensions.[31−33] This increase in molecular ordering is due to the well-documented side-chain interdigitation observed between adjacent lamellae in PBTTT.[13,28] Because of this increased molecular ordering, BTTT oligomers were chosen as a model system to study the relationship between their molecular, electronic, and, morphological properties as well as their cocrystallization with fullerenes.[34−37]

Herein, we report the synthesis and characterization of monomeric through pentameric BTTT. The crystallization and cocrystallization of PCBM with increasing molecular weight is of particular focus. We note that, in the case of BTTT-2, the presence of PCBM alters the stacking of the BTTT-2 sheets in such a way that discrete one-dimensional (1D) channels are formed that perfectly host the fullerene molecules. This increased orientational order in BTTT-2 brought about by PCBM is also observed in coarse-grained molecular simulations of neat BTTT-2 and BTTT-2/PCBM blends. The influence of molecular, electronic, and morphological properties of these oligomers on device performance is characterized.

RESULTS AND DISCUSSION

Synthesis and Electronic Structure. In general, the chain length of monodisperse oligomers was elongated by stepwise cross-coupling of two asymmetric monomers to both ends of a symmetric bifunctional core. The synthetic steps to oligomers and polymer are shown in Scheme 1. For example, the trimer was synthesized via a palladium-catalyzed Stille reaction between monobrominated and distannylated monomers. For the longer oligomers (n = 4, 5), the key intermediates are monobrominated dimers, which are prepared in reasonable yield by treatment of the dimer with *N*-bromosuccinimide (NBS) in chloroform at room temperature. Additionally, we used the dibrominated monomer as a building block to

dx.doi.org/10.1021/ja510976n | J. Am. Chem. Soc. 2014, 136, 18120−18130

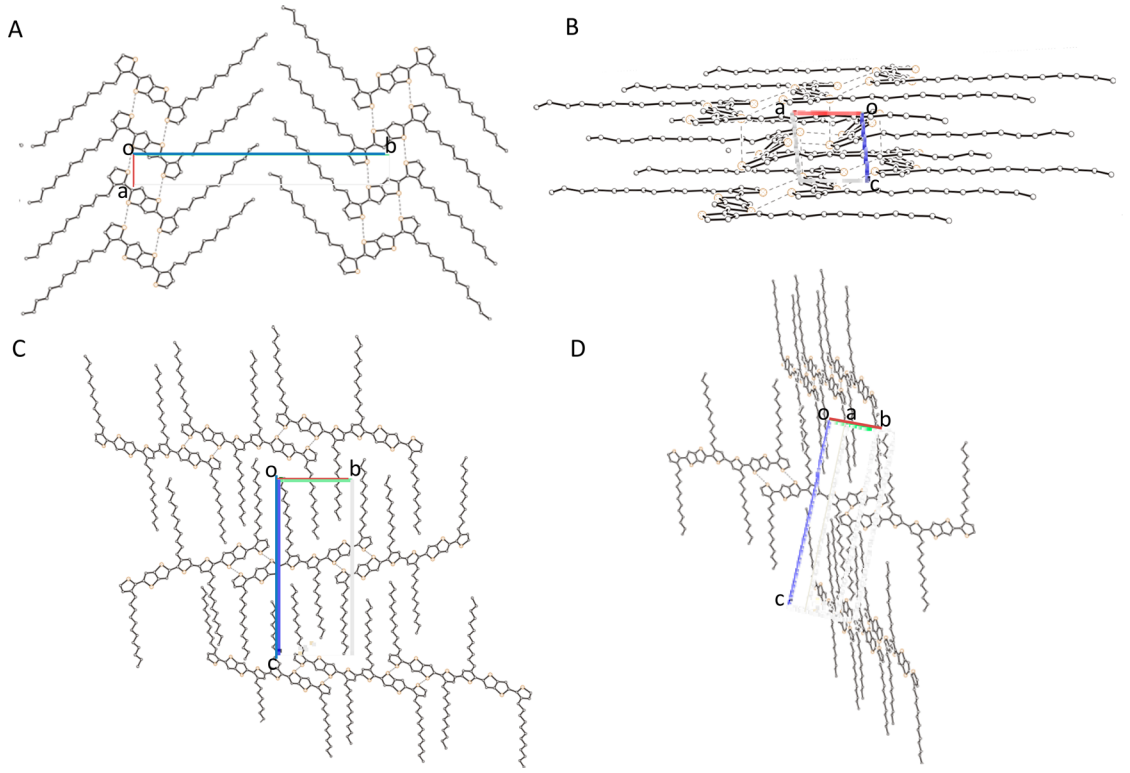

Figure 2. (A) Crystal packing of BTTT-1 along the *c*-axis. (B) Intermolecular interactions of BTTT-1 along the *b*-axis with S···S interactions. (C) Crystal packing of BTTT-2 along the *a*-axis and intermolecular interactions. (D) Crystal packing of BTTT-2 with "rotated" layer (plane angle of 48°).

synthesize low molecular weight PBTTT, which was purified by solvent extraction (chloroform) and afforded a mixture of tetramer, pentamer, and hexamer with a polydispersity index (PDI) of 1.44 (labeled as BTTT-C from here on). A detailed description of the synthesis is available in Supporting Information.

The desired oligomers exhibit excellent solubility in common solvents, such as chloroform, tetrahydrofuran (THF), and toluene, and were readily purified by silica column chromatography and recrystallization in hexane with more than hundreds of milligram batches. The molecular structures of all oligomers were unambiguously characterized by matrix-assisted laser desorption/ionization time-of-flight (MALDI-TOF) and ^{1}H NMR spectroscopy. The molecular weights of the oligomers as measured by gel-permeation chromatography (GPC) increased proportionately with increasing thiophene units in the oligomeric series and were overestimated by a factor of 1.80 relative to the MALDI-TOF measurements (Figure 1A,B). This is due to the use of polystyrene (PS) standards for GPC and indicates that the backbones of the oligomers are rodlike in conformation.[17] The high molecular weight polymer (PBTTT) was synthesized as described previously, with M_n of 30 000 g/mol and PDI of 1.80.[28]

Figure 1C shows the absorption of the oligothiophenes in chloroform. As expected, the absorption spectra undergo bathochromic shifts with increasing molecular weight due to the extended conjugation length. The difference in λ_{max} between BTTT-4 and BTTT-5 is 1 nm, indicating that the conjugation saturates at or above BTTT-5.[25] However, the spectra are broad and featureless with little change in shape, indicating a lack of inter- or intramolecular coupling. In general, there are continuous red shifts of the absorption spectra in the solid state compared to in solution due to more planar conformations and stronger interchain interactions (see Supporting Information). However, BTTT-1 displays large blue shifts in the solid state, suggesting H-aggregation.[24,38] The ionization potential (IP), that is, the oxidation onset, was measured between 5.39 and 4.90 eV and the first oxidation potentials gradually decreased to saturation with increasing chain length (see Supporting Information). Optical gaps obtained from the absorption onsets vary from 2.99 to 2.21 eV.

Structure Analysis, Crystal Packing, and Film Morphology. Although the crystal packing models of PBTTT have been developed by combination of experimental X-ray diffraction (XRD) and computational calculation, detailed information along the backbone and side chains, such as intermolecular interactions, torsion angles, and positioning of the alkyl chains, is rather limited.[33,36] To investigate how the chain length affects the solid-state structures of oligothiophenes, single crystals of BTTT-1 and BTTT-2 were obtained from slow evaporation of a hexane solution and analyzed by X-ray diffraction. Figure 2A,B shows the intermolecular interactions and packing motif of BTTT-1 as viewed along *c*- and *b*- axes. This compound is slightly twisted, and the dihedral angle between the outer thiophene ring and thienothiophene ring is about 12° (Supporting Information). All the thiophene rings exhibit an anti conformation with pendant long alkyl chains extended perpendicular to the backbone. Along the *a*-axis, the molecules are stacked into two nonequivalent stacks with the alkyl chains perpendicular to each other. Therefore, there is no alkyl chain interdigitation observed. In each stack, the two S atoms in the thienothiophene unit are linked to two S atoms in outer thiophene rings of adjacent molecules, and the

dx.doi.org/10.1021/ja510976n | J. Am. Chem. Soc. 2014, 136, 18120−18130

stacks are held together by a network of multiple S···S interactions.

In crystals of BTTT-2, the eight α-linked rings in the backbone exhibit anti conformations, and the maximum torsion angle between the thiophene and the thienothiophene rings is close to 14.0° (Figure 2C,D; Supporting Information). The backbones interact with each other via close S···S and S···H contacts. Interestingly, the $a-b$ plane sheets in this crystal structure are stacked in an ABA fashion with the interlayered B sheets rotated by about 48° relative to the A sheets. This stacking and rotation angle can be understood by analyzing the possibilities for efficient interdigitation of the B-sheet alkyl chains in the channels formed by the upright BTTT-2 side chains from the A sheet. Without rotation, the B-sheet chains would not make would "good use" of the channel space (single chain per channel), but two chains that roughly occupy the $^1/_3$ and $^2/_3$ places in the gap of length L (see also schematic in Figure 3) fill this space efficiently and require the ~48° rotation

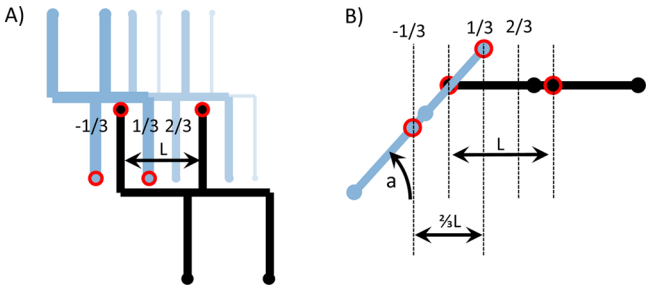

Figure 3. Model structure of the interlayered $a-b$ sheet (blue) rotated with respect to the base (black) sheet: (A) side view and (B) top view. The rotation angle α under which this is accomplished can be calculated from $\cos(\alpha) = (^2/_3L)/L = {}^2/_3$, α = 48.19°, and is in perfect agreement with the measured angle.

of B sheets relative to A sheets. A number of intermolecular S···H interactions are observed between the different A and B sheets. Within a given sheet, the $\pi\cdots\pi$ distance is close to 3.4 Å.

For BTTT-3, the attempts to grow high-quality crystals for structure analysis by X-rays were unsuccessful. Nevertheless, X-ray diffraction data show that the unit cell is triclinic, with unit cell parameters a = 9.58 Å, b = 12.45 Å, c = 22.87 Å, α = 90.50°, β = 98.77°, and γ = 100.46°.

To further investigate how conjugation length influences the packing structure and unit cell parameters of the oligomers, grazing incidence X-ray diffraction (GIXD) scattering was performed on thin-film samples. Figure 4 shows the GIXD scattering patterns of BTTT films as cast on bare Si substrates. In Figure 4A it can be seen that BTTT-1 exhibits a "2D powder" texture wherein crystalline grains are oriented parallel to the substrate but randomly distributed azimuthally, something that is common for thin polycrystalline films of small organic molecules. From the peak positions in the diffraction pattern, the crystal unit cell was indexed, with unit cell parameters a = 7.604 Å, b = 7.561 Å, c = 32.976 Å, α = 85.74°, β = 83.61°, and γ = 97.22°. These values are fairly similar to those of the bulk unit cell with the exception that the d_{010} spacing of the BTTT-1 thin-film phase (~33 Å) is close to half that of the corresponding bulk single-crystal spacing (64 Å). This indicates that the crystal packing in BTTT-1 thin film exhibits a higher degree of symmetry than that in the bulk crystal, with fewer molecules in the unit cell and correspondingly shorter lamellar stacking distance.

The BTTT-2 diffraction images show a significantly lower degree of ordering than those of the BTTT-1 films; fewer, broader peaks with a wider angular spread indicates that the BTTT-2 grains are less well aligned with respect to the substrate surface. The d_{001} spacing of BTTT-2 thin-film phase (22 Å) is also approximately half that of the corresponding single-crystal spacing (42 Å) as in the BTTT-1 case, suggesting again that crystalline packing is more efficient in thin film than in bulk in the lamellar stacking direction.

We note that while the BTTT-1 and BTTT-2 diffraction images were indexed in accordance with the successfully obtained bulk unit cells, we labeled the peaks in the diffraction images of BTTT-3 following the scheme that is most commonly used for semicrystalline polythiophenes such as P3HT or PBTTT: the lamellar stacking axis is chosen as first lattice axis and the h Miller indices label the out-of-plane diffraction peaks. The lamellar stacking peaks in BTTT-3 scattering patterns, that is, (h00) peaks, correspond to a stacking distance of about 18.6 Å, which is shorter than the corresponding value of the bulk crystal (22.87 Å), suggesting a

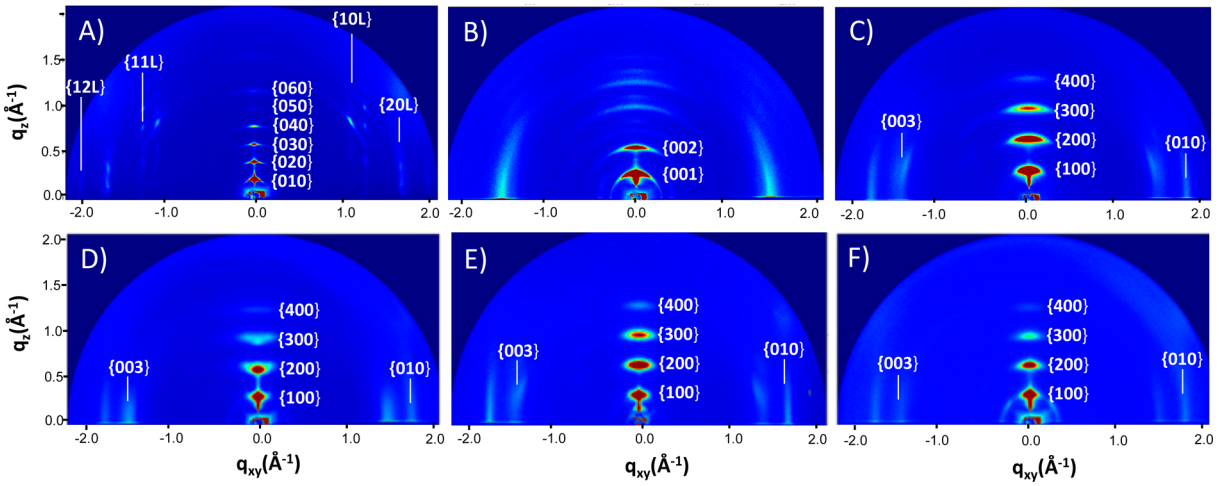

Figure 4. GIXD images of oligothiophenes on spun on bare Si from chlorobenzene: (A) BTTT-1, (B) BTTT-2, (C) BTTT-3, (D) BTTT-4, (E) BTTT-5, and (F) BTTT-C.

dx.doi.org/10.1021/ja510976n | J. Am. Chem. Soc. 2014, 136, 18120−18130

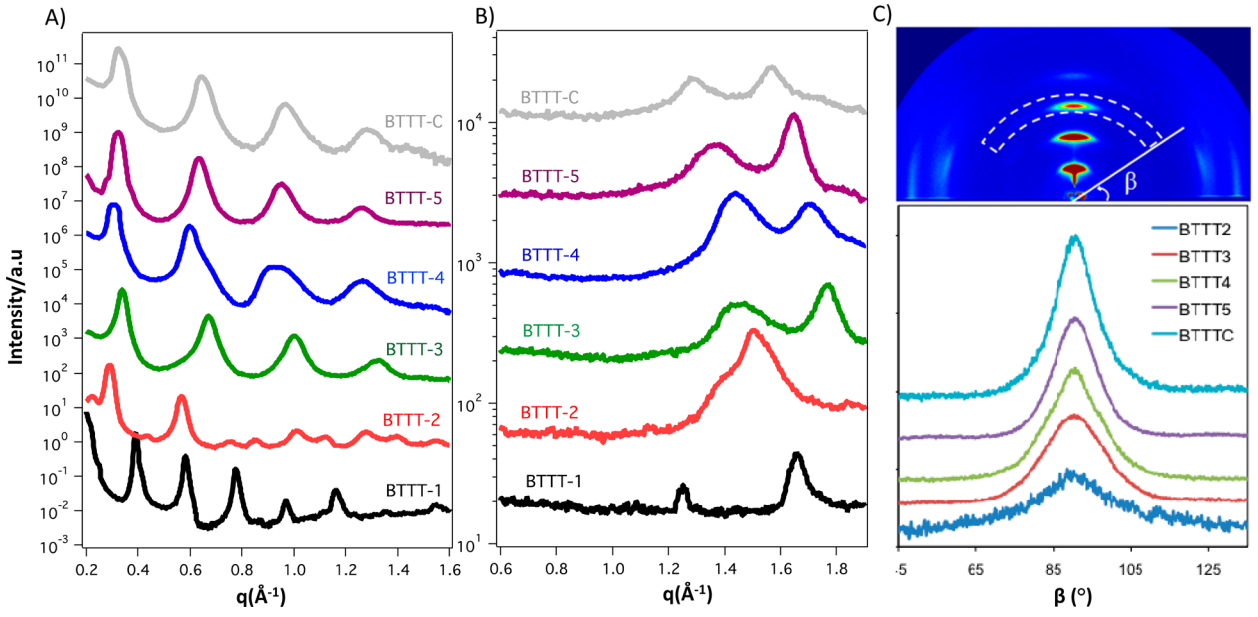

Figure 5. (A) Out-of-plane and (B) in-plane diffraction plots from GIXD patterns of BTTT oligomers. (C) Approximate pole figures of (300) Bragg reflection as a function of BTTT oligomers.

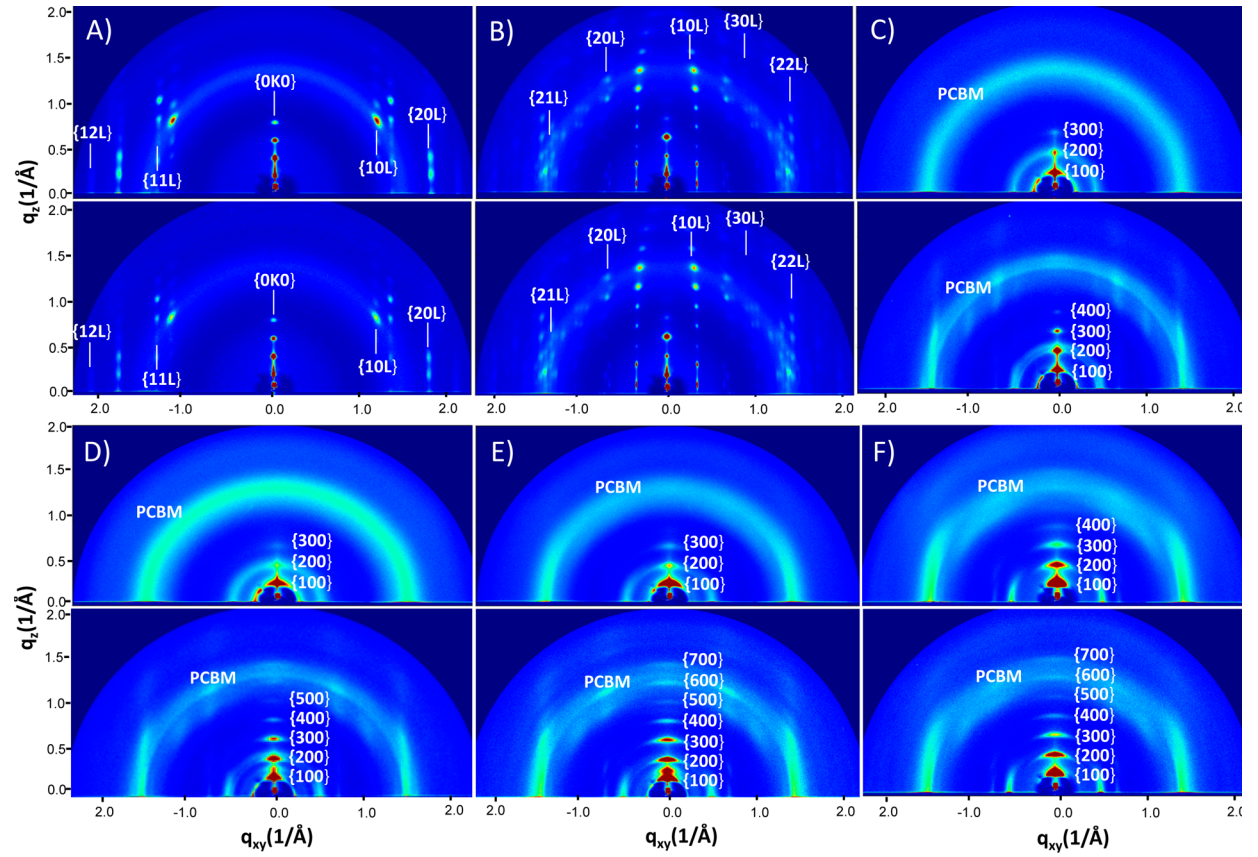

Figure 6. GIXD scattering images of BTTT/fullerene blends (1:1 w/w). Top, as-cast; bottom, annealed. (A) BTTT-1, (B) BTTT-2, (C) BTTT-3, (D) BTTT-4, (E) BTTT-5, and (F) BTTT-C.

possibly greater extent of alkyl-chain interdigitation in the thin film. The in-plane peak located at q_{xy} = 1.40 Å^{-1} matches closely with that of high molecular weight PBTTT and can be indexed as (003), where (001) would correspond to the repeat unit length of the oligomer of 12.28 Å. Again, by analogy with other common polythiophenes, the peak at q_{xy} = 1.70 Å^{-1} can be labeled (010), which would correspond to a $\pi-\pi$ stacking distance of 3.70 Å.[12]

The diffraction pattern of BTTT-4 films is quite similar to that of BTTT-3 films but shows an increase of lamellar stacking distance d_{100} to 21.0 Å and straighter, more vertical in-plane peaks 1.40 and 1.70 Å^{-1}. The straighter peaks indicate that

dx.doi.org/10.1021/ja510976n | J. Am. Chem. Soc. 2014, 136, 18120−18130

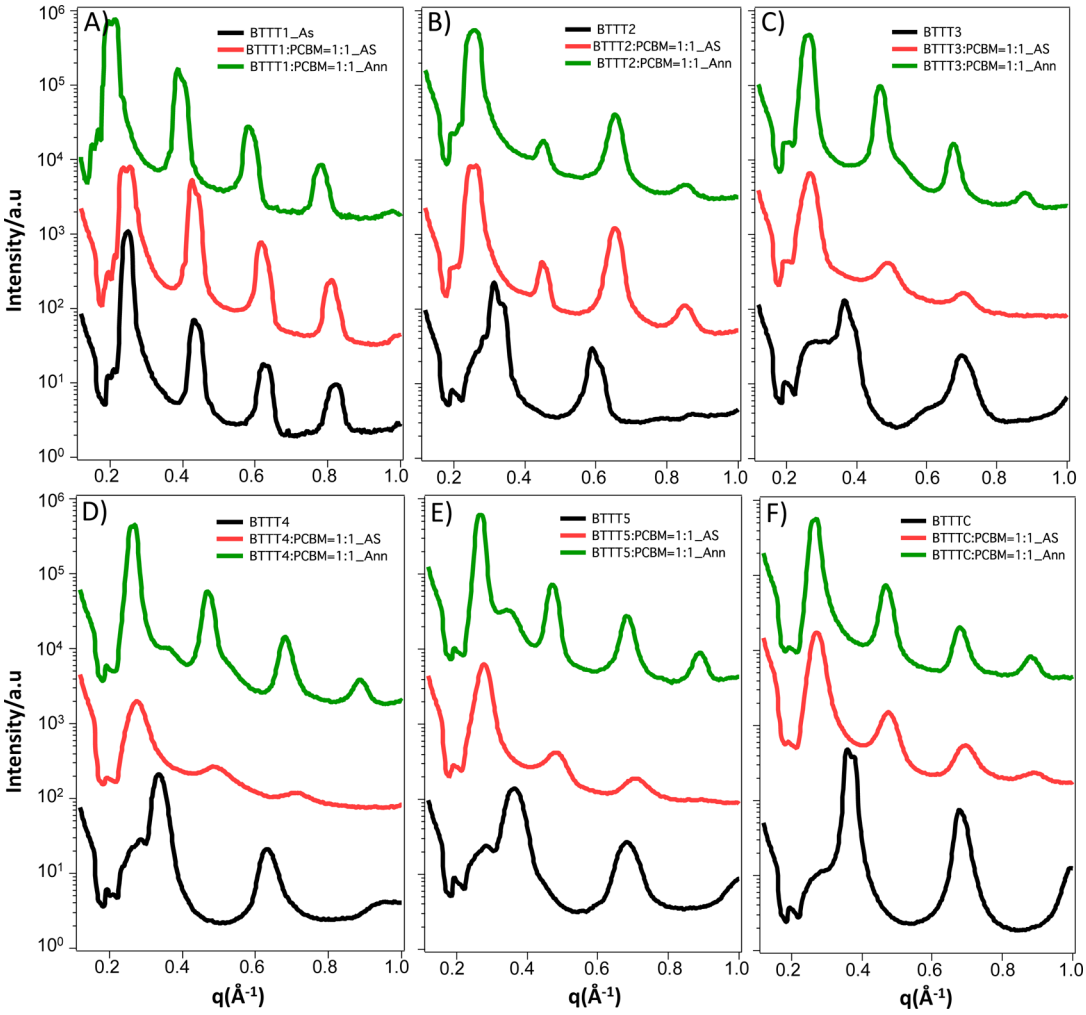

Figure 7. Out-of-plane diffraction plots from GIXD patterns of BTTTs and BTTT/PCBM blends (1:1 w/w).

there is a better registry between BTTT-4 grains and the substrate surface. The difference in d_{100} spacing suggests that BTTT-3 and BTTT-4 exhibit different degrees of alkyl interdigitation. Recently, Northrup[39] reported the relationship between alkyl chain interdigitation and crystal stability of PBTTT. On the basis of those results, the d_{100} spacings of ∼16 and ∼34.0 Å indicate full alkyl-chain interdigitation and minimal interdigitation, respectively. This is possibly due to the difference in symmetry; BTTT-4 has a lower molecular symmetry with respect to its side chains than BTTT-3, which likely allows for a more dense molecular packing motif.[24]

Diffraction patterns of thin films of BTTT-5 and BTTT-C are nearly identical to that of PBTTT and the d_{100} spacing is about 19.6 Å, which indicates side-chain interdigitation. Unit-cell parameters of BTTT-5 and BTTT-C are also very similar to those of PBTTT.[36] From the GIXD images, it is apparent that higher molecular weight oligomers and the polymer order in nearly the same way on the substrate and share the same packing motif. Since interaction between adjacent backbones and interdigitation between neighboring alkyl chains are the dominant factors in deciding the molecular packing, increasing the backbone length beyond the pentamer does not significantly change the intermolecular packing. The most significant changes in the diffraction patterns, and consequently the molecular packing, occur between the monomer and the trimer. The only clear trend going from BTTT-3 to BTTT-5 and further to BTTT-C is an improvement in the registration of grains with substrate.

To examine how the molecular weight affected the crystal orientation (Figure 5C), we used the (300) peak to estimate the crystal orientation distribution.[40] The (300) peak exhibits an angular full width at half-maximum (fwhm) of 24.8°, 20.2°, 16.9°, 14.3°, and 12.4° for BTTT-2 to BTTT-C, respectively; the angular spread of the peak decreased with increasing molecular weight, indicating that the crystalline domains become more aligned out-of-plane with the increase in molecular weight. BTTT-1 exhibits good device performance, with mobility up to 3×10^{-3} $cm^2 \cdot V^{-1} \cdot s^{-1}$. However, thin-film transistors of BTTT-2 show mobility of 10^{-4} $cm^2 \cdot V^{-1} \cdot s^{-1}$, and the low mobility can be attributed to the crossed stacks in the crystal packing of BTTT-2, which is unfavorable for charge transport. We observed that increasing the molecular weight from BTTT-3 to BTTT-5 lead to an increasing mobility from 0.002 to 0.01 $cm^2 \cdot V^{-1} \cdot s^{-1}$. BTTT-C with medium molecular weight showed mobilities in the range 0.018−0.025 $cm^2 \cdot V^{-1} \cdot s^{-1}$, which are comparable to that of high molecular weight PBTTT without annealing (see Supporting Information).[28]

Intermolecular Intercalation of BTTT/Fullerene Blends. The performance of bulk heterojunction (BHJ) solar cells is known to heavily depend on the interpenetrating nanostructure formed by donor and acceptor components.[41,42] It has been reported that fullerenes intercalate into the side

dx.doi.org/10.1021/ja510976n | J. Am. Chem. Soc. 2014, 136, 18120−18130

chains of PBTTT to form highly ordered bimolecular crystals.[43−46] To acquire the influence of conjugation length on the crystalline behavior of the mixture of donor and acceptor, GIXD experiments were performed on thin films of 1:1 BTTT/PCBM blends (Figure 6). In the case of BTTT-1/PCBM blends, the scattering pattern is similar to that of the pristine thin films even though it is overall more defined. The unit cell of a = 7.604 Å, b = 7.561 Å, c = 32.976 Å, α = 85.74°, β = 83.61°, and γ = 97.22° is very similar to the bulk unit cell of BTTT-1. It is likely that the trans conformation of two alkyl side chains prevents incorporation of the fullerene molecules into the BTTT-1 lattice, and there is no shift observed in the d-spacing for the blend BTTT-1/PCBM (Figures 7 and 8).

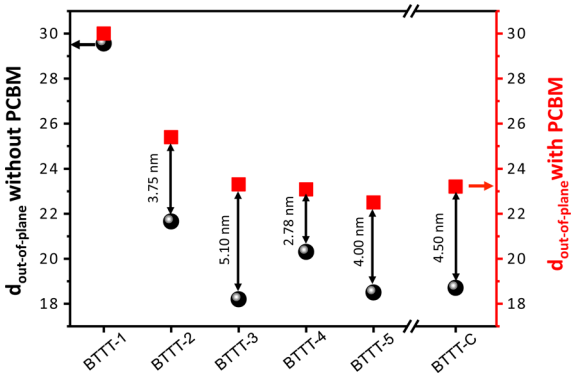

Figure 8. Out-of-plane distance vs oligothiophene length before and after blending with PCBM.

In contrast to the pristine BTTT-2 films, the BTTT-2/PCBM blend films show much sharper peaks and significantly improved crystallinity. This hints at the fact that PCBM "catalyzes" a more efficient packing of the BTTT-2 dimers. The diffraction peaks of the blend film are aligned vertically (indicating that the crystalline grains are aligned with the substrate plane). From these Bragg rods, a subset can be indexed with unit cell a = 4.931 Å, b = 17.973 Å, c = 30.923 Å, α = 73.898°, β = 98.389°, and γ = 89.685° that is similar to the bulk and has a virtually identical a−b plane as the bulk. The corresponding c-vector is significantly shorter than in the BTTT-2 bulk crystal, indicating that the rotated interlayer from the full bulk unit cell is gone in the thin film. If, on the basis of virtually identical a−b plane geometry, we assume that BTTT-2 packing in the a−b plane sheets is not substantially changed from the bulk, stacking the a−b plane bulk sheets with the new c-vector forms a BTTT-2 assembly with straight grooves or gaps (Figure. 9A,B) that could easily accommodate PCBM molecules.

More importantly, since the above BTTT-2 unit cell explains only a portion of the diffraction peaks, the remaining spots in Figure 6B have to be attributed to a sublattice of PCBM. We were able to successfully index a PCBM lattice with unit cell a = 9.580 Å, b = 18.012 Å, c = 31.007 Å, α = 72.616°, β = 82.633°, and γ = 93.800°, which explains all missing spots and which on the other hand shares many peaks with the BTTT-2 lattice, a fact that very strongly points to the formation of a cocrystal in the BTTT-2/PCBM blend films. The short axis of the PCBM unit cell is very close to the minimum distance at which PCBM molecules can be stacked, indicating that they form 1D channels along the a-axis direction (Figure 9C; see Supporting Information). Figure 9D shows our structural model in which the PCBM sublattice unit cell contains two PCBM molecules. This sublattice fits perfectly into the channels formed by the BTTT-2 molecules in the blend film unit cell, yielding a molecular cocrystal and assembly that contains PCBM structures that should facilitate very efficient electron transport. We also note that, in the present case, the PCBM molecules cannot be located in between BTTT-2 aromatic chains since the BTTT-2's a−b plane in the blend films (which contains the stacking direction of the aromatic backbones) would have then been different from the BTTT-2 bulk crystal. The channels, formed by the BTTT-2 side-chain interdigitation and backbone S···S and π···π interactions, can efficiently accommodate the linear PCBM sublattice. This is different from the proposed structure for PBTTT/$PC_{71}BM$ cocrystal thin films.[46] This packing-wise efficient and likely energy-lowering assembly between the two materials is most certainly also responsible for the significant improvement in the BTTT-2/PCBM blend film's overall crystallinity relative to that of the BTTT-2 films.

Calculated structures of BTTT-2/PCBM blends and of neat BTTT-2 as obtained from molecular simulations using coarse-grained models developed by Jayaraman and co-workers[47,48] also show an increased orientational ordering of BTTT-2 in the presence of PCBM as compared to pristine BTTT-2 with no PCBM (Figure 10). We note that the generic coarse-grained models used in these molecular dynamics (MD) simulations were validated in earlier work on thiophene-based oligomers[47,48] and were *not* customized to reproduce any of the experimental data in this paper (see Supporting Information for details of the model and simulation protocol). Therefore, it is striking that, in agreement with the experimental results, these independently validated MD simulations also predict higher orientational order. This is quantified by the orientational order parameter $P_2(r)$ of BTTT-2 backbone−backbone distances, which is larger in the blends with PCBM than in pristine systems in the absence of PCBM (Figure 10b). The PCBM molecules are found to intercalate between the side chains of BTTT-2 in the ordered state. The favorable enthalpic interactions between PCBM and BTTT-2, in addition to the favorable attractive (stacking) interactions between the (red) beads of orientationally aligned BTTT-2 backbones and the favorable topology of BTTT-2 that allows the PCBMs to intercalate, together lower the total energy of the ordered states of BTTT-2/PCBM over the neat BTTT-2 systems at similar temperature and pressure. Such PCBM intercalation was not observed with this model in blends of PCBM with oligomers of poly(3-hexyl thiophene)[47] or with BTTT-1/PCBM blends, the latter showing a different packing motif compared to BTTT-2/PCBM blends (data not shown).

Going beyond BTTT-2, even though there were not enough peaks visible in the diffraction images for the longer BTTT/PCBM blends to create a structural model as detailed as that for BTTT-2/PCBM, a shorter d-spacing as seen in the case of BTTT-2/PCBM was observed for all blends with BTTT-3 and longer oligomers, as shown in Figures 6 and 8. The (0k0) and (00l) scattering intensities at the q_{xy} axis that belong to pristine BTTT films disappear in blended films. We attribute the decrease in stacking distance to a similar situation as in the BTTT-2 case: an efficient intercalation of PCBM molecules in gaps or channels between the side chains of the oligomers, which produces bimolecular crystals that are lower in energy than those with an additional interlayer, rotated a−b plane sheet. Although thermal annealing does not significantly affect the peak positions, the diffraction peak intensity increased with

dx.doi.org/10.1021/ja510976n | J. Am. Chem. Soc. 2014, 136, 18120−18130

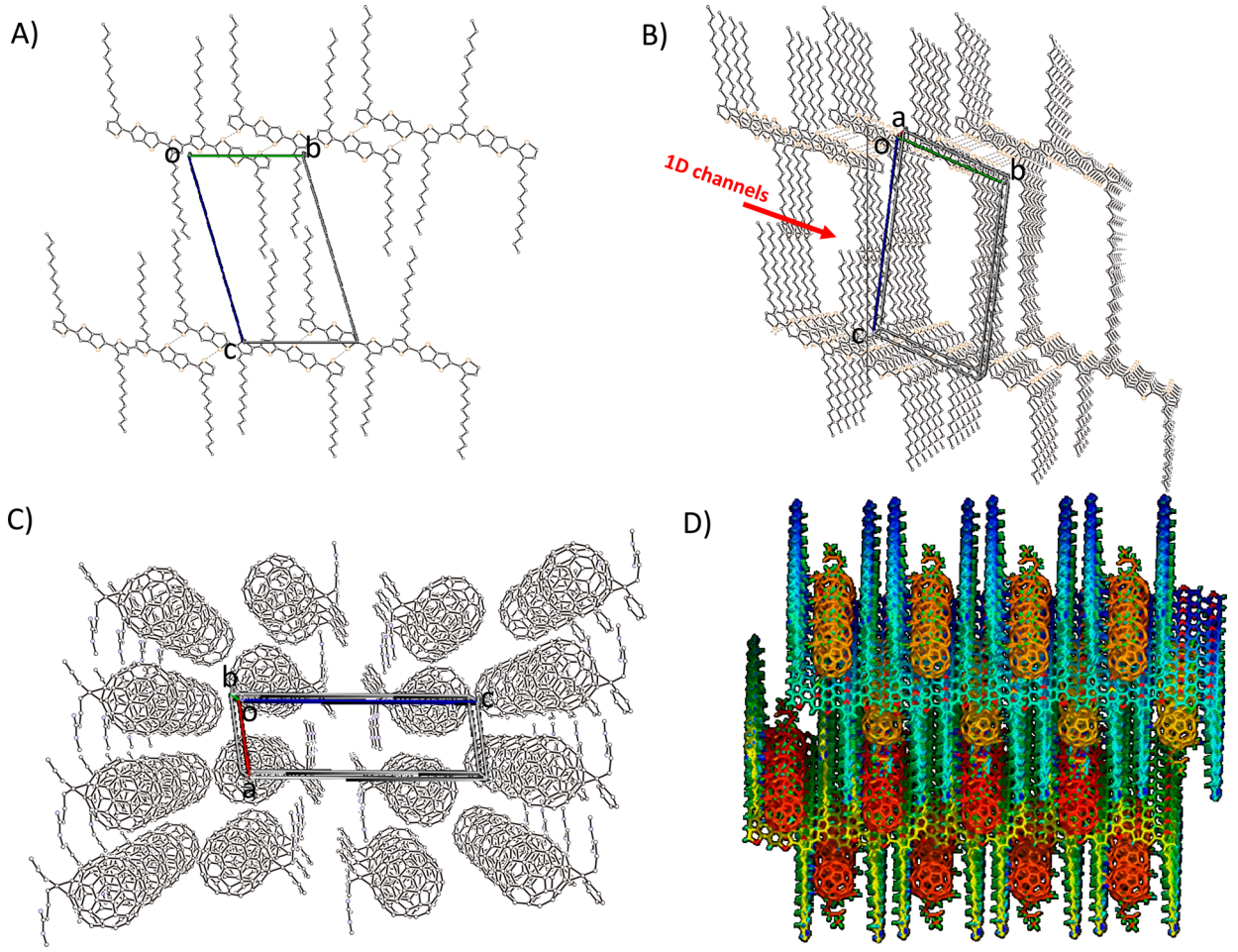

Figure 9. (A) Crystal packing of BTTT-2 "catalyzed" by PCBM. (B) 1D channels formed by BTTT-2 side chains. (C) Crystal packing of PCBM. (D) Bimolecular cocrystal packing of BTTT-2/PCBM (the channels host PCBMs).

annealing temperature (Figures 6 and 7). This suggests that the bimolecular crystals are thermodynamically stable and that crystallinity is enhanced through thermal treatment.

Photovoltaic Properties of BTTT Oligomer–Fullerene Blends. Photovoltaic properties of the oligomers were measured in BHJ solar cells with $PC_{71}BM$ as the complementary electron acceptor. The device structure was ITO/PEDOT–PSS (30 nm)/[oligomers/$PC_{71}BM$ (~100 nm)]/LiF (1.5 nm)/Al. The current density–voltage (J–V) characteristics of the solar cells under simulated AM 1.5 solar illumination at 100 mW·cm^{-2} light intensity are shown in Supporting Information. The BHJ solar cells were fabricated by spin-coating a solution of oligomers and $PC_{71}BM$ (1:4) in chloroform, resulting in an active layer with a thickness of 100 nm (complementary polymer PBTTT/$PC_{71}BM$ blend photovoltaic devices were also fabricated, with 1,2-dichlorobenzene as the processing solvent). Figure 11 shows open-circuit voltage (V_{oc}), short-circuit current density (J_{sc}), fill factor (FF), and power conversion efficiency (PCE) as a function of molecular weight. These data are summarized in Table 1.

In 1:1 BTTT/$PC_{71}BM$ films (see Supporting Information), the intercalation of fullerene into the side chains of these oligomers prohibited the formation of a continuous electron pathway, which significantly reduced the electron transport, although excitons were quenched efficiently.[49] Therefore, the 1:1 BTTT/$PC_{71}BM$ films had very low power conversion efficiency due to their low short circuit current. As the ratio of fullerene was increased up to 1:4, the excess $PC_{71}BM$ formed pure aggregated domains (as seen from the $PC_{71}BM$ diffraction rings in GIXD), and their percolation led to continuous pathways for electron transport. Thus, the J_{sc} and PCE of 1:4 BTTT/$PC_{71}BM$ blended devices are orders of magnitude higher than for 1:1 blends. The best device performance was for PBTTT-based solar cells with an average J_{sc} = 7.07 mA/cm^2, V_{oc} = 0.43 V, FF = 54%, and PCE = 1.63%. The PCE is comparable with that of PBTTT-C_{14} reported by McGehee and co-workers.[43] On the contrary, the device based on BTTT-1 showed J_{sc} = 0.45 mA/cm^2, V_{oc} = 0.74 V, FF = 22%, and PCE = 0.07%, due to limited absorption in the visible region. Interestingly, the device based on BTTT-2 showed much better performance with J_{sc} = 3.74 mA/cm^2, V_{oc} = 0.84 V, and FF = 28%, thus improving the PCE up to 0.9%. The V_{OC} gradually decreases from 0.85 V for BTTT-2 to 0.4 V for PBTTT, which may be ascribed to the increasing highest occupied molecular orbital (HOMO) energy. Similar behavior is also observed in poly(3-butylthiophene) (P3BT) system.[50] It seems that the variations in V_{oc} could depend more on the intrinsic frontier orbital energy level of the oligomers than on the degree of microstructural order of the blended thin films. With increasing molecular weight from BTTT-2 to BTTT-5, a slight decrease in J_{sc} is observed from 3.74 to 2.18 mA/cm^2. This can be attributed to the unique stacking of the BTTT-2 film as observed in the GIXD. However, from BTTT-C to PBTTT, there is a more significant increase in J_{sc} from 2.92 to

dx.doi.org/10.1021/ja510976n | J. Am. Chem. Soc. 2014, 136, 18120–18130

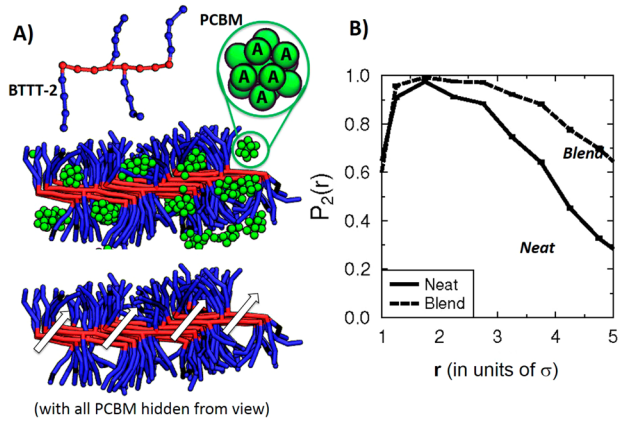

Figure 10. (A) Simulation snapshot of a section of the simulation box showing PCBM molecules (inset shows a single PCBM molecule, modeled as the green icosahedral collection of coarse-grained "type A" spheres) intercalating amidst the side chains of BTTT-2. Bottom image shows the same snapshot as above with PCBM molecules hidden from view to present clearly the channels formed by side chains to host the PCBM, as suggested in experiments. (B) Orientational order parameter between BTTT-2 backbones, P_2, as a function of r, defined as the distance between centers of mass of BTTT-2 backbones in reduced units of σ (where σ = 0.3 nm) show higher orientational order (higher P_2) of BTTT-2 in blends versus neat systems, especially at larger r. See Supporting Information for description of the $P_2(r)$ calculation.

7.07 mA/cm^2, which is due to the better connectivity of the PBTTT domains. The PCE is observed to slowly decrease with increasing conjugation length in the low molecular weight region but increase with increasing conjugation length in the high molecular weight region.

Table 1. Photovoltaic Parameters of Bulk Heterojunction Solar Cells Based on the Blend of Oligomers and $PC_{71}BM$ (1:4 w/w)

oligomers	V_{oc} (V)	J_{sc} (mA/cm^2)	FF (%)	PCE (%)
BTTT-1	0.74 (0.031)	0.45 (0.202)	22 (2.0)	0.07 (0.032)
BTTT-2	0.84 (0.041)	3.74 (0.510)	28 (1.5)	0.89 (0.175)
BTTT-3	0.74 (0.007)	3.51 (0.705)	29 (1.6)	0.77 (0.182)
BTTT-4	0.64 (0.015)	2.20 (0.369)	29 (1.6)	0.41 (0.079)
BTTT-5	0.55 (0.005)	2.18 (0.513)	31 (0.9)	0.37 (0.079)
BTTT-C	0.52 (0.018)	2.92 (0.410)	34 (4.2)	0.51 (0.042)
PBTTT	0.43 (0.008)	7.07 (0.901)	54 (1.9)	1.63 (0.207)

Resonant soft X-ray scattering was used to probe the morphological features of these blended thin films (Supporting Information).[40,51] For the oligomer thin-film blends, we cannot see obvious phase separations; the scattering intensity decays smoothly without measurable features. The slight upturn in the low-q region is likely a result of the thickness/roughness variations of the films, and its size scale is out of the functional size region for efficient OPVs. This poor morphology led to relatively small current and fill factor in devices. In the PBTTT-based thin films, the 1:4 blends showed improved morphology as indicated from a broad hump in the RSoXS profile, relating to a broad range of phase separation sizes. This led to the sharply enhanced current and fill factor in devices.

CONCLUSION

We synthesized a series of monodisperse oligothiophenes based on 2,5-bis(3-alkylthiophen-2-yl)thieno[3,2-*b*]thiophene

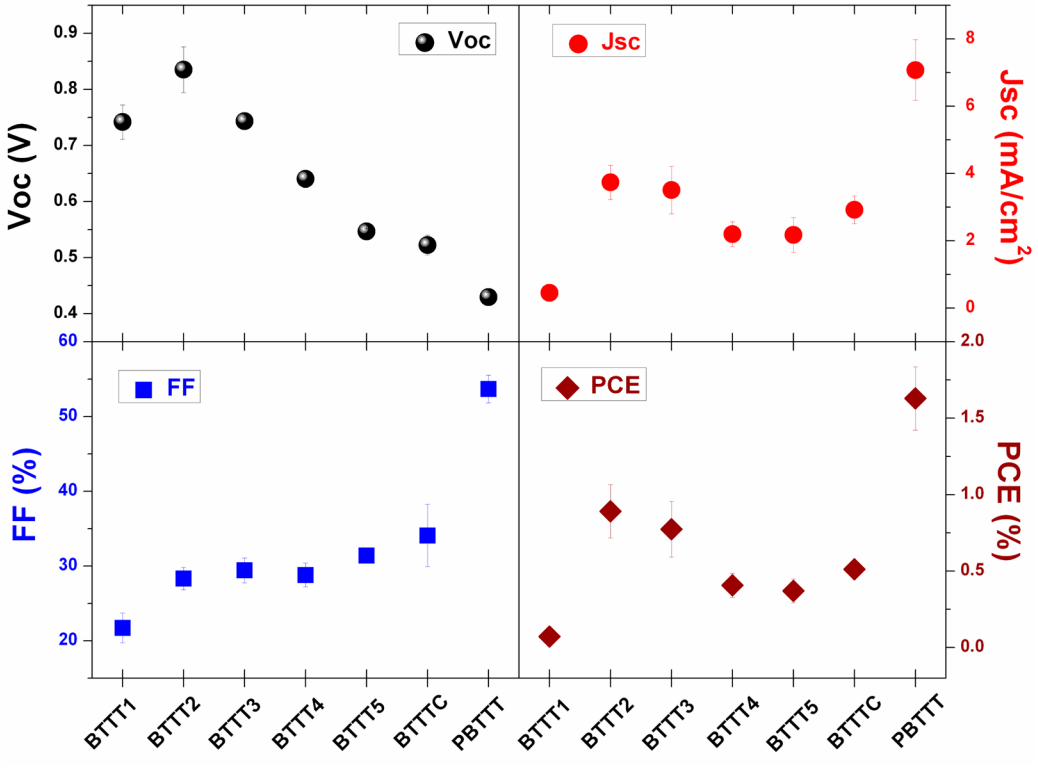

Figure 11. Characteristics of solar cells with oligomers and $PC_{71}BM$ (1:4 w/w) as active layers as a function of thiophene units: open-circuit voltage (V_{oc}), short-circuit current density (J_{sc}), fill factor (FF), and power conversion efficiency (PCE).

dx.doi.org/10.1021/ja510976n | J. Am. Chem. Soc. 2014, 136, 18120−18130

(BTTT) and thoroughly investigated their thin-film morphology and crystallinity by GIXD. Analysis of their molecular structure revealed that the longer oligomers, particularly BTTT-3 and BTTT-5, adopt a crystal packing that is expected to be commensurate with the polymer, PBTTT. In contrast to the proposed structure in the case of PBTTT/$PC_{71}BM$, the PCBM reorganizes BTTT-2 to form 1D channels, seen in both experiments and molecular simulations. This particular feature is due to the unstable "rotated" layers in neat BTTT-2 thin films, which have weak intermolecular interactions between adjacent layers. This is the first time oligothiophene crystallization has been shown to be catalyzed by PCBM to form 1D channels. Also noteworthy is that the actual sublattice of PCBM was determined by X-ray crystallography. Furthermore, intercalation of PCBM is observed beyond BTTT-2 oligomers, likely similar to that of PBTTT, and no phase separation is observed in 1:1 blends. This work demonstrates that oligomers can be used as model systems for their polymer counterparts and other conjugated polymers.

■ ASSOCIATED CONTENT

Ⓢ Supporting Information

Additional text, 22 figures, and four tables giving detailed synthesis and characterization of the oligomers; ^{1}H and ^{13}C NMR spectra of the oligomers; crystal data for BTTT-1 and BTTT-2; DSC, UV, and CV spectra; and model and simulation method details (PDF). Four crystallographic files for BTTT-1, BTTT-2, BTTT-2(catalyzed), and PCBM sublattice (CIF). This material is free of charge via the Internet at http://pubs.acs.org.

■ AUTHOR INFORMATION

Corresponding Authors

Stefan.Mannsfeld@tu-dresden.de
abriseno@mail.pse.umass.edu

Author Contributions

[Δ]L.Z. and F.L. contributed equally.

Notes

The authors declare no competing financial interest.

■ ACKNOWLEDGMENTS

L.Z. and A.L.B thank the National Science Foundation (DMR-1112455) and the Office of Naval Research (N0001471410053). Financial support for F.L. and T.P.R. and spectroscopic characterization was carried out using facilities supported as part of Polymer-Based Materials for Harvesting Solar Energy, an Energy Frontier Research Center funded by the U.S. Department of Energy, Office of Basic Energy Sciences under Award DE-SC000108. S.C.B.M. acknowledges partial support by the German Research Foundation (DFG) within the Cluster of Excellence "Center for Advancing Electronics Dresden". Y.D. acknowledges initial support from a seed grant by the Department of Energy, Laboratory Directed Research and Development funding, under Contract DE-AC02-76SF00515 and subsequent support by the Department of Energy, Bridging Research Interactions through Collaborative Development Grants in Energy (BRIDGE) program under Contract DE-FOA-0000654-1588. X-ray experiments were carried out at the Stanford Synchrotron Radiation Lightsource, a national user facility operated by Stanford University on behalf of the U.S. Department of Energy, Office of Basic Energy Sciences. H.S.M. and A.J. thank the U.S. Department of Energy, Office of Basic Energy Sciences (Grant DE-SC0003912) for financially supporting the simulations presented in this work and acknowledge the use of supercomputing resources at National Energy Research Scientific Computing Center supported by the Office of Science of the U.S. Department of Energy under Contract DE-AC02-05CH11231.

■ REFERENCES

(1) Mishra, A.; Ma, C.-Q.; Bäuerle, P. *Chem. Rev.* **2009**, *109*, 1141−1276.
(2) McCullough, R. D. *Adv. Mater.* **1998**, *10*, 93−116.
(3) *Electronic Materials: The Oligomer Approach*; Müllen, K., Wenger, G., Eds.; Wiley−VCH,: Weinheim, Germany, 1997.
(4) *Handbook of Thiophene-Based Materials: Applications in Organic Electronics and Photonics*; Perepichka, I. F., Perepichka, D. F., Eds.; Wiley: Chichester, U.K., 2009.
(5) Capozzi, B.; Dell, E. J.; Berkelbach, T. C.; Reichman, D. R.; Venkataraman, L.; Campos, L. M. *J. Am. Chem. Soc.* **2014**, *136*, 10486−10492.
(6) Beaujuge, P. M.; Fréchet, J. M. J. *J. Am. Chem. Soc.* **2011**, *133*, 20009−20029.
(7) Thompson, B. C.; Fréchet, J. M. J. *Angew. Chem., Int. Ed* **2007**, *47*, 58−77.
(8) Zen, A.; Saphiannikova, M.; Neher, D.; Grenzer, J.; Grigorian, S.; Pietsch, U.; Asawapirom, U.; Janietz, S.; Scherf, U.; Lieberwirth, I.; Wegner, G. *Macromolecules* **2006**, *39*, 2162−2171.
(9) Kline, R. J.; McGehee, M. D.; Toney, M. F. *Nat. Mater.* **2006**, *5*, 222−228.
(10) Kline, R. J.; McGehee, M. D.; Kadnikova, E. N.; Liu, J. S.; Fréchet, J. M. J. *Adv. Mater.* **2003**, *15*, 1519−1522.
(11) Prosa, T. J.; Winokur, M. J.; Moulton, J.; Smith, P.; Heeger, A. J. *Macromolecules* **1992**, *25*, 4364−4372.
(12) Kline, R. J.; McGehee, M. D.; Kadnikova, E. N.; Liu, J. S.; Fréchet, J. M. J.; Toney, M. F. *Macromolecules* **2005**, *38*, 3312−3319.
(13) Kline, R. J.; Delongchamp, D. M.; Fischer, D. A.; Lin, E. K.; Richter, L. J.; Chabinyc, M. L.; Toney, M. F.; Heeney, M.; McCulloch, I. *Macromolecules* **2007**, *40*, 7960−7965.
(14) Zen, A.; Pflaum, J.; Hirschmann, S.; Zhuang, W.; Jaiser, F.; Asawapirom, U.; Rabe, J. P.; Scherf, U.; Neher, D. *Adv. Funct. Mater.* **2004**, *14*, 757−764.
(15) Lim, J. A.; Liu, F.; Ferdous, S.; Muthukumar, M.; Briseno, A. L. *Mater. Today* **2010**, *13*, 14−24.
(16) Takimiya, K.; Sakamoto, K.; Otsubo, T.; Kunugi, Y. *Chem. Lett.* **2006**, *35*, 942−943.
(17) Izumi, T.; Kobashi, S.; Takimiya, K.; Aso, Y.; Otsubo, T. *J. Am. Chem. Soc.* **2003**, *125*, 5286−5287.
(18) Mena-Osteritz, E.; Meyer, A.; Langeveld-Voss, B. M. W.; Janssen, R. A. J.; Meijer, E. W.; Bäuerle, P. *Angew. Chem., Int. Ed* **2000**, *39*, 2679−2684.
(19) Bäuerle, P.; Fischer, T.; Bildlingmeier, B.; Stabel, A.; Rabe, J. *Angew. Chem. Int. Ed* **1995**, *34*, 303−307.
(20) Koch, F. P. V.; Smith, P.; Heeney, M. *J. Am. Chem. Soc.* **2013**, *135*, 13695−13698.
(21) Azumi, R.; Götz, G.; Debaerdemaeker, T.; Bäuerle, P. *Chem.—Eur. J.* **2000**, *6*, 735−744.
(22) Azumi, R.; Mena-Osteritz, E.; Boese, R.; Benet-Buchholz, J.; Bäuerle, P. *J. Mater. Chem.* **2006**, *16*, 728−735.
(23) Fichou, D. *J. Mater. Chem.* **2000**, *10*, 571−588.
(24) Zhang, L.; Colella, N. S.; Liu, F.; Trahan, S.; Baral, J. K.; Winter, H. H.; Mannsfeld, S. C. B.; Briseno, A. L. B. *J. Am. Chem. Soc.* **2013**, *135*, 844−854.
(25) Zhang, L.; Colella, N. S.; Cherniawski, B. P.; Mannsfeld, S. C. B.; Briseno, A. L. *ACS Appl. Mater. Interfaces* **2014**, *6*, 5327−5343.
(26) Osaka, I.; McCullough, R. D. *Acc. Chem. Res.* **2008**, *41*, 1202−1214.
(27) Zhang, R.; Li, B.; Lovu, M. C.; Jeffries-EL, M.; Sauvé, G.; Cooper, J.; Jia, S.; Tristram-Nagle, S.; Smilgies, D. M.; Lambeth, D. N.;

McCullough, R. D.; Kowalewski, T. *J. Am. Chem. Soc.* **2006**, *128*, 3480−3481.
(28) McCulloch, I.; Heeney, M.; Bailey, C.; Genevicius, K. J.; MacDonald, I.; Shkunov, M.; Sparrowe, D.; Tierney, S.; Wagner, R.; Zhang, W.; Chabinyc, M. L.; Kline, R. J.; McGehee, M. D.; Toney, M. F. *Nat. Mater.* **2006**, *5*, 328−333.
(29) Hamadani, B. H.; Gundlach, D. J.; McCulloch, I.; Heeney, M. *Appl. Phys. Lett.* **2007**, *91*, No. 243512.
(30) Wang, S.; Kiersnowski, A.; Pisula, W.; Müllen, K. *J. Am. Chem. Soc.* **2012**, *134*, 4015−4018.
(31) Brocorens, P.; Vooren, A.; Chabinyc, M. L.; Toney, M. F.; Shkunov, M.; Heeney, M.; McCulloch, I.; Cornil, J.; Lazzaroni, R. *Adv. Mater.* **2009**, *21*, 1193−1198.
(32) McCulloch, I.; Heeney, M.; Chabinyc, M. L.; deLongchamp, D.; Kline, R. J.; Cölle, M.; Duffy, W.; Fischer, D.; Gundlach, D.; Hamadani, B.; Hamilton, R.; Richter, L.; Salleo, A.; Shkunov, M.; Sparrowe, D.; Tierney, S.; Zhang, W. *Adv. Mater.* **2009**, *21*, 1091−1009.
(33) Chabinyc, M. L.; Toney, M. F.; Kline, R. J.; McCulloch, I.; Heeney, M. *J. Am. Chem. Soc.* **2007**, *129*, 3226−3237.
(34) Delongchamp, D. M.; Kline, R. J.; Lin, E. K.; Fischer, D. A.; Richter, L. J.; Lucas, L. A.; Heeney, M.; McCulloch, I.; Northrup, J. E. *Adv. Mater.* **2007**, *19*, 833−837.
(35) Himmelberger, S.; Dacuňa, J.; Rivnay, J.; Jimison, L. H.; McCarthy-Ward, T.; Heeney, M.; McCulloch, I.; Toney, M. F.; Salleo, A. *Adv. Funct. Mater.* **2013**, *23*, 2091−2098.
(36) Cho, E.; Risko, C.; Kim, D.; Gysel, R.; Miller, N. C.; Breiby, D. W.; McGehee, M. D.; Toney, M. F.; Kline, R. J.; Brédas, J.-L. *J. Am. Chem. Soc.* **2012**, *134*, 6177−6190.
(37) Gasperini, A.; Sivula, K. *Macromolecules* **2013**, *46*, 9349−9358.
(38) Zhang, L.; Tan, L.; Wang, Z.; Hu, W.; Zhu, D. B. *Chem. Mater.* **2009**, *21*, 1993−1999.
(39) Northrup, J. E. *Phys. Rev. B* **2007**, *76*, No. 245202.
(40) Rivnay, J.; Mannsfeld, S. C. B.; Miller, C. E.; Salleo, A.; Toney, M. F. *Chem. Rev.* **2012**, *112*, 5488−5519.
(41) Dang, M. H.; Hirsch, L.; Wantz, G.; Wuest, J. D. *Chem. Rev.* **2013**, *113*, 3734−3765.
(42) Coughlin, J. E.; Henson, Z. B.; Welch, G. C.; Bazan, G. C. *Acc. Chem. Res.* **2014**, *47*, 257−270.
(43) Cates, N. C.; Gysel, R.; Beiley, Z.; Miller, C. E.; Toney, M. F.; Heeney, M.; McCulloch, I.; McGehee, M. D. *Nano. Lett.* **2009**, *9*, 4153−4157.
(44) Cates, N. C.; Sweetnam, S.; Hoke, E. T.; Gysel, R.; Miller, C. E.; Bartelt, J. A.; Xie, X.; Toney, M. F.; McGehee, M. D. *Nano. Lett.* **2012**, *12*, 1566−1570.
(45) Mayer, A. C.; Toney, M. F.; Scully, S. R.; Rivnay, J.; Brabec, C. J.; Scharber, M.; Koppe, M.; Heeney, M.; McCulloch, I.; McGehee, M. D. *Adv. Funct. Mater.* **2009**, *19*, 1173−1179.
(46) Miller, N. C.; Cho, E.; Junk, M. J. N.; Gysel, R.; Risko, C.; Kim, D.; Sweetnam, S.; Miller, C. E.; Richter, L. J.; kline, J.; Heeney, M.; McCulloch, I.; Amassian, A.; Acevedo-Feliz, D.; Knox, C.; Hansen, M.; Dudenko, D.; Chmelka, B. F.; Toney, M. F.; Brédas, J.-L.; McGehee, M. D. *Adv. Mater.* **2012**, *24*, 6071−6079.
(47) Jankowski, E.; Marsh, H. S.; Jayaraman, A. *Macromolecules* **2013**, *46*, 5775−5785.
(48) Marsh, H. S.; Jankowski, E.; Jayaraman, A. *Macromolecules* **2014**, *47*, 2736−2747.
(49) Buchaca-Domingo, E.; Ferguson, A. J.; Jamieson, F. C.; McCarthy-Ward, T.; Shoaee, S.; Tumbleston, J. R.; Reid, O. G.; Yu, L.; Madec, M. B.; Pfannmöller, M.; Hermerschmidt, F.; Schröder, R. R.; Watkins, S. E.; Kopidakis, N.; Portale, G.; Amassian, A.; Heeney, M.; Ade, H.; Rumbles, G.; Durrant, J. R.; Stingelin, N. *Mater. Horiz.* **2014**, *1*, 270−279.
(50) Hiorns, R. C.; Bettignies, R.; Leroy, J.; Bailly, S.; Firon, M.; Sentein, C.; Khoukh, A.; Preud'homme, H.; Dagron-Lartigau, C. *Adv. Funct. Mater.* **2006**, *16*, 2263−2273.
(51) Ade, H.; Stoll, H. *Nat. Mater.* **2009**, *8*, 281−290.